Barrier Selection Rules for Quantum Dots-in-a-Well Infrared Photodetector

Ajit V. Barve, *Student Member, IEEE*, Saumya Sengupta, Jun Oh Kim, John Montoya, Brianna Klein, Mohammad Ali Shirazi, *Student Member, IEEE*, Marziyeh Zamiri, Yagya D. Sharma, *Senior Member, IEEE*, Sourav Adhikary, Sebastián E. Godoy, Woo-Yong Jang, Glauco R. C. Fiorante, Subhananda Chakrabarti, *Member, IEEE*, and Sanjay Krishna, *Senior Member, IEEE*

***Abstract*— We report on a systematic study of the effect of barriers on quantum dots-in-a-well infrared photodetectors. Four devices are fabricated and characterized with varying composition for barriers adjacent to quantum dots and away from quantum dots. Effects of these "proximity" and "remote" barriers are studied by comparing photoluminescence, responsivity, dark current, background-limited operating temperature, activation energy, and detectivity. The growth mechanism for a conformal coverage of quantum dots with proximity barriers is described and supported with reflection high-energy electron diffraction and transmission electron microscopy images. It is shown that proximity barriers and remote barriers influence the characteristics of the detector very differently, with increases in proximity barrier energy leading to higher responsivity and lower dark current, while remote barriers reduce the responsivity and dark currents simultaneously. It is demonstrated that confinement enhancing barriers as proximity barriers optimize the SNR at low bias range, suitable for focal plane array applications.**

***Index Terms*— Barriers, confinement enhancing barriers quantum dots, quantum dots in a well (DWELL).**

I. Introduction

QUANTUM dot infrared photodetectors (QDIP) [1]–[5], have been actively studied in the last few years due to their potential for high operating temperature imaging [6], drawing from the already established quantum well infrared photodetector (QWIP) technology. However, it is hard to control the peak detection wavelengths in QDIPs due to the sensitivity of growth of Stranski-Krastanov (SK) quantum dots on growth parameters [7]. Quantum dots-in-a-well (DWELL) architecture [8]–[14] in which, typically, InAs (or InGaAs) quantum dots are embedded in InGaAs-GaAs quantum well or InGaAs-GaAs-AlGaAs double quantum well [15], provides a viable alternative to traditional QDIP designs. DWELL architecture allows better material growth characteristics and the ability to precisely and predictably control the peak wavelengths just by changing the composition and dimensions of quantum wells. Characteristics of DWELL detectors, such as responsivity, spectral response, dark current, photoconductive gain etc are highly dependent, and hence tunable, on the details of barrier designs and growth characteristics. In this paper, important relationships between these characteristics to barrier design parameters will be discussed.

DWELL detectors with AlGaAs barriers provide several excited states in the conduction band, leading to a bias tunable multicolor operation [14], [16], [17]. For high operating temperatures, the most important requirement is low dark current, such that charge wells in readout integrated circuits (ROIC) are not saturated. In traditional DWELL designs, however, there is a tradeoff between the dark current level, the responsivity and the peak wavelength. For example, if the AlGaAs barrier energy increases, the dark current level drops exponentially, but the escape probability of the photoexcited, bound electrons also decreases, leading to a decrease in the responsivity. Since longwave infrared (LWIR) carriers are bound deep inside, they cannot escape at low bias levels, thus limiting the maximum detection wavelength. Other effect is increase in the optimal operating bias [2], [12], [16], [18], with the increase in AlGaAs barrier energy. Since typical ROIC bias levels are limited to low values, these designs are not well suited for FPA imaging.

It has been previously demonstrated [19] that bound to quasibound (B-Q) type of transitions, in which the infrared absorption takes place between a bound state in quantum dot and a quasibound state very close to the barrier conduction band energy, optimizes the detectivity at moderate bias, leading to high operating temperatures [20]. These transitions combine the advantages of bound to continuum (B-C) transitions, such as, high escape probability, low bias operation

Manuscript received April 16, 2012; revised June 26, 2012; accepted July 5, 2012. Date of publication July 13, 2012; date of current version July 27, 2012. This work was supported in part by AFRL FA9453-12-1-0336 and KRISS GRL Program and in part by the Department of Science and Technology, India.

A. V. Barve is with the Center for High Technology Materials, University of New Mexico, Albuquerque, NM 87106 USA, and also with the Department of Electrical and Computer Engineering, University of California, Santa Barbara, CA 93106 USA (e-mail: ajitvb1@gmail.com).

S. Sengupta, S. Adhikary, and S. Chakrabarti are with the Center for Excellence in Nanoelectronics, Department of Electrical Engineering, Indian Institute of Technology Bombay, Mumbai 400076, India (e-mail: saumyasengupta2002@gmail.com; sourav.ism@gmail.com; subhanandachakrabarti@gmail.com).

J. O. Kim, J. Montoya, B. Klein, M. A. Shirazi, M. Zamiri, Y. D. Sharma, W.-Y. Jang, G. R. C. Fiorante, and S. Krishna are with the Center for High Technology Materials, University of New Mexico, Albuquerque, NM 87106 USA (e-mail: jokim@chtm.unm.edu; redshift@unm.edu; turtlefood122@gmail.com; mali@unm.edu; marziyeh.zamiri@gmail.com; yagya@chtm.unm.edu; wjang@ece.unm.edu; glauco@unm.edu; skrishna@chtm.unm.edu).

S. E. Godoy is with the Center for High Technology Materials, University of New Mexico, Albuquerque, NM 87106 USA, and also with the Departamento de Ingeniería Eléctrica, Universidad de Concepción, Concepción 160-C, Chile (e-mail: sgodoy@unm.edu).

Color versions of one or more of the figures in this paper are available online at http://ieeexplore.ieee.org.

Digital Object Identifier 10.1109/JQE.2012.2208621

0018–9197/$31.00 © 2012 IEEE

with those of bound to bound (B-B) types of transitions, such as high absorption quantum efficiency. Performance of B-Q type of transitions can be further improved with confinement enhanced (CE) barriers [21]. CE DWELL detectors have been previously demonstrated [21] to increase the responsivity and decrease the noise, simultaneously, for a low bias operation, thus increasing the signal to noise ratio (SNR).

There are several design parameters in the design of DWELL devices for FPA applications, such as the absolute values of dark current and responsivity, the spectral range, detectivities and the optimum operating bias. In this work, we perform a series of systematic experiments in order to understand the tradeoff associated with different barrier configurations for optimizing these parameters. We compare the characteristics of CE DWELL detectors with different traditional barrier compositions and spacing to examine the device design rules for optimizing the signal to noise ratio at a lower bias. Four devices were designed and fabricated with different 'proximity barriers', which are barriers adjacent to the DWELL region and 'remote barriers' which are thick barriers separating the DWELL regions to avoid strain coupling and inter-dot tunneling. CE DWELL designs have been shown to optimize the SNR at lower bias amongst the four devices.

II. Device Designs

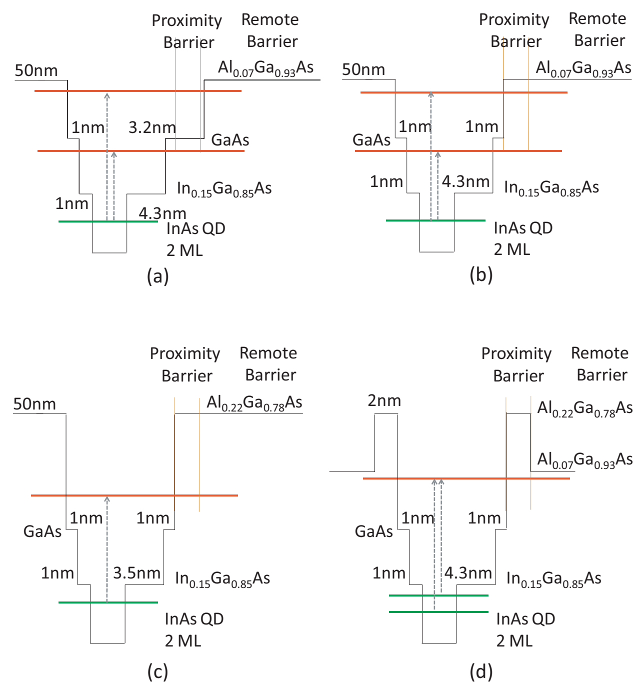

Fig. 1. Schematic conduction band diagram for (a) device A, (b) device B, (c) device C and (d) device D, showing the thicknesses, composition of various materials used, and approximate position of the ground-state and excited-state energies of interest. Primary transitions, corresponding to peaks in the spectral response are also marked. The diagrams are not to scale.

Fig. 1(a)–(d) shows the schematics of four devices (A, B, C and D) designed for this study. Only the locations of the ground state energy levels of quantum dots and confined state energy levels in quantum wells are shown. These energies are extracted with a semi-empirical approach, based on the photocurrent spectra, photoluminescence (PL) data and known conduction band offsets between the materials. In all the devices, InAs quantum dots with 2 monolayer (ML) nominal thickness are embedded in $In_{0.15}Ga_{0.85}As$ quantum well. Quantum dots are doped such that there are approximately 2 electrons per dot. Quantum wells and quantum dots are grown at 500 °C and barrier regions are grown at 590 °C. All the devices have 7 stacks of DWELL, each separated by 50 nm thick barrier regions and sandwiched between n-doped contact regions. In device A, B and D, the 50 nm thick barrier separating the DWELL regions, here onwards called 'remote barrier' is $Al_{0.07}Ga_{0.93}As$, while in device C this barrier is composed of $Al_{0.22}Ga_{0.78}As$. In device A, B and D, $In_{0.15}Ga_{0.85}As$ quantum well thickness is 1nm below the quantum dot (strain bed) and 4.3 nm above the quantum dot (strain cap). In device C, the strain cap thickness was lowered to 3.5 nm, keeping the strain bed at 1 nm, in order to increase the escape probability of the electrons due to increase in the excited state energy.

Growth temperature changes are facilitated by growing 1 nm GaAs layer after the growth of remote barrier at high temperature and growing 1 nm GaAs after the strain cap at 500 °C, to avoid Indium desorption from the quantum well. We define the term 'proximity barrier' as the 2 nm region grown directly after the growth of 1 nm GaAs layer after the quantum well. Thus, in Device A, the proximity barrier is GaAs, in Device B, the proximity barrier is composed of $Al_{0.07}Ga_{0.93}As$, while in Device C and D it is $Al_{0.22}Ga_{0.78}As$. In device D, the proximity barrier serves as confinement enhancing barrier. Table I summarizes compositions of different barriers in all the devices. Temperature is ramped up after the growth of GaAs layer during a 3 minute long growth interruption. During this period, the excess InAs is evaporated off, leading to uniform height distribution and flat top quantum dots. This is important, as it assures that the barrier layers are grown on top of quantum dots. Therefore, it is clear that the InAs quantum dots are embedded within CE-barriers in device D, resulting in the effect of barrier in transverse direction. This can be justified by looking at reflection high energy electron diffraction (RHEED) pattern during the growth of the active region, as shown in Fig. 2.

Fig. 2(a) shows the chevron-type RHEED pattern, typical of SK quantum dots. Fig. 2(b) shows spotty RHEED pattern during the InGaAs capping, indicating that the quantum dots are not yet fully covered, which changes to a streak pattern during the GaAs capping layer growth. After this capping layer, during the temperature ramping, the pattern shows sharp lines, thus indicating that the excess Indium has been evaporated from larger quantum dots which are not fully covered by the capping layer. This insures that the CE-barriers are grown over the quantum dots.

The conformal coverage of the CE barriers over the quantum dots was also confirmed with transmission electron microscopy (TEM). Fig. 3 shows some of the images obtained with sample D. Fig. 3(a) shows all the seven stacks with quantum dots. Excellent material quality with no visible defect can be observed. The quantum dot density is almost constant in all

TABLE I

SUMMARY OF COMPOSITIONS OF BARRIERS AND MEASURED ELECTRICAL PROPERTIES OF ALL THE STRUCTURES

Device	Proximity barrier	Remote barrier	Wavelength range (μm)	Optimal bias (V)	Responsivity at –0.4 V (77 K) (mA/W)	Dark current at –0.4 V (77 K) (A/cm^2)	Peak detectivity (77 K) ($cm.Hz^{1/2}W^{-1}$)
A	GaAs	$Al_{0.07}Ga_{0.93}As$	4–11	$\pm 0.2-0.8$	10	3.9×10^{-5}	2.7×10^{9}
B	$Al_{0.07}Ga_{0.93}As$	$Al_{0.07}Ga_{0.93}As$	5–11	$\pm 0.3-1$	40	1.6×10^{-4}	6.8×10^{9}
C	$Al_{0.22}Ga_{0.78}As$	$Al_{0.22}Ga_{0.78}As$	5–8	$\pm 2.5-3.5$	0.3	$<10^{-11}$ (system limited)	1.4×10^{11}
D	$Al_{0.22}Ga_{0.78}As$	$Al_{0.07}Ga_{0.93}As$	5–9	$\pm 0.4-1.2$	77	3.2×10^{-5}	7.3×10^{10}

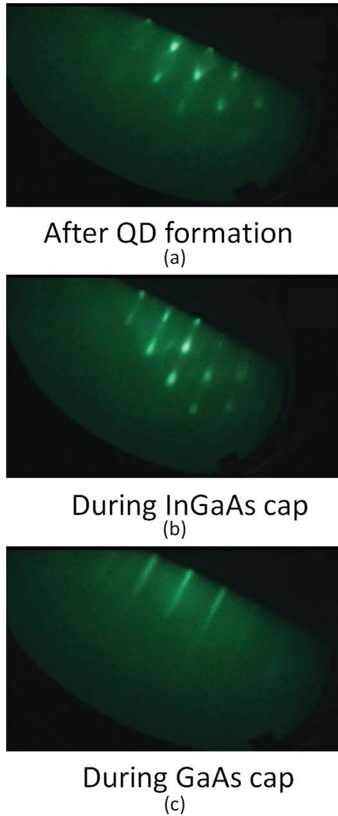

Fig. 2. RHEED patterns during the growth of different layers. (a) Chevron pattern after the quantum dot growth. (b) Spotty pattern during the capping layer growth, indicating partially capped quantum dots. (c) Streak pattern during the GaAs capping layer growth, indicating that the quantum dots are completely covered and the surface is flat.

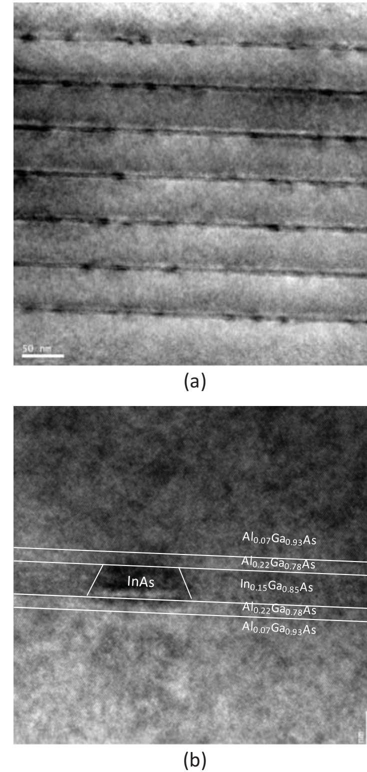

Fig. 3. TEM images of device D. (a) All seven stacks showing excellent material quality and dot uniformity. (b) Flat-top pyramidal quantum dot in a compressively strained InGaAs quantum well.

the seven layers. Fig. 3(b) shows the expanded view of one of the quantum dots. A flat-top pyramidal quantum dots, with the base width of 16–18 nm and the height of 7 nm, along with a compressively strained $In_{0.15}Ga_{0.85}As$ quantum well is clearly visible. CE-barriers can be seen above and below the quantum well as bright stripes, although the contrast between $Al_{0.07}Ga_{0.93}As$ and $Al_{0.22}Ga_{0.78}As$ layers in this strain field map is low. Strain fields from the quantum dots above and below the quantum dots are visible.

III. RESULTS

After the MBE growth, photoluminescence measurement was done on with He-Ne laser at room temperature. Fig. 4 shows the normalized PL from all four devices. The peak of PL was found at 1154 nm (Device A), 1142 nm (Device B), 1076 nm (Device C) and 1118 nm (Device D). Clearly, as the Al concentration in the proximity barrier increase, e.g. GaAs for device A, $Al_{0.07}Ga_{0.93}As$ for device B and $Al_{0.22}Ga_{0.78}As$ in device C and D, the PL wavelength is blue-shifted. This is not only because of the increase in confinement due to barrier action, but could also be because Aluminum acts as a mechanical diffusion barrier, reducing the loss of confinement due to In to Ga interdiffusion, resulting in smaller quantum dots. Between device C and D, device C has lower PL peak wavelength due to a smaller strain cap thickness, resulting in smaller quantum dots. Interestingly, the PL intensity follows the same trend as PL wavelength, as it highest for device A and lowest for device C. This is due to interfacial defects caused by the

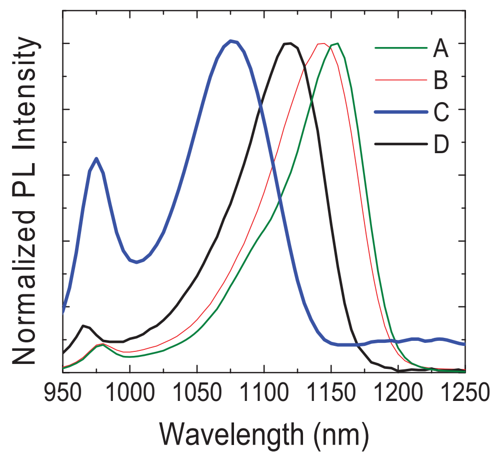

Fig. 4. Normalized PL spectra of all four devices measured using He–Ne laser at room temperature. Reduction in the peak wavelength is attributed to lowering of interdiffusion due to mechanical barrier action of Al. Device C has lower PL peak wavelength due to lower strain cap thickness above the quantum dot.

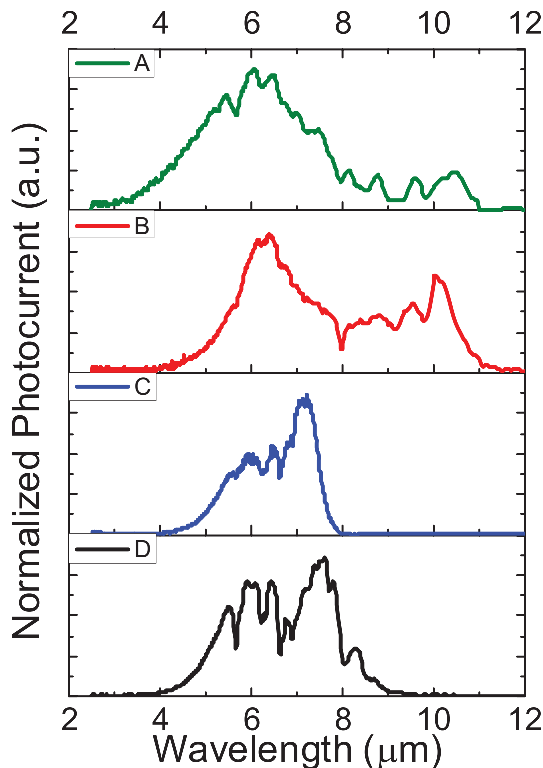

Fig. 5. Spectral response from the four devices at 77 K. The 10- to 10.5-μm peak present in devices A and B is absent in devices C and D due to the presence of Al0.22Ga0.78As barrier, which blocks long-wavelength carriers.

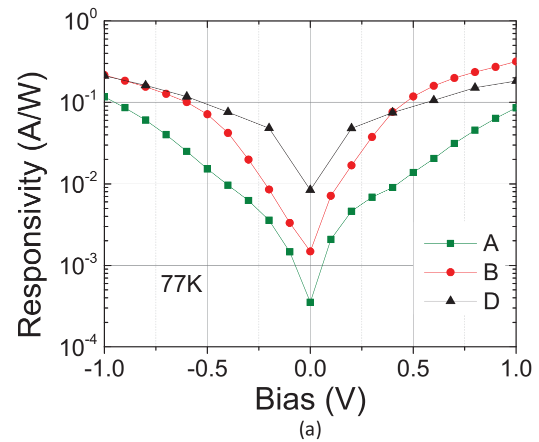

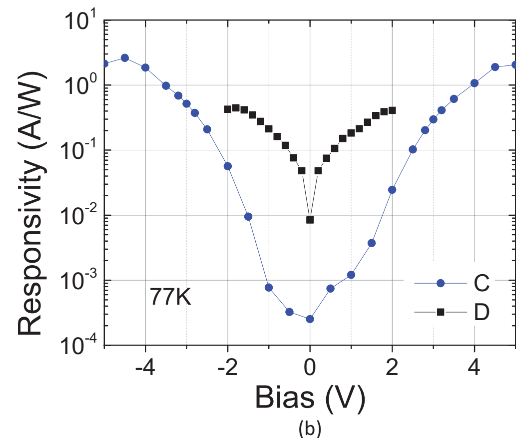

Fig. 6. (a) Effect of proximity barrier on the responsivity. Devices A, B, and D have same remote barrier. It is clear that as the proximity barrier energy increases, the responsivity increases due to better confinement in the excited state leading to a higher wavefunction overlap with the ground state. (b) Effect of remote barrier on the responsivity is much more drastic, with several orders of magnitude reduction in the responsivity due to the blocking of both photocarriers and dark current carriers by a large barrier.

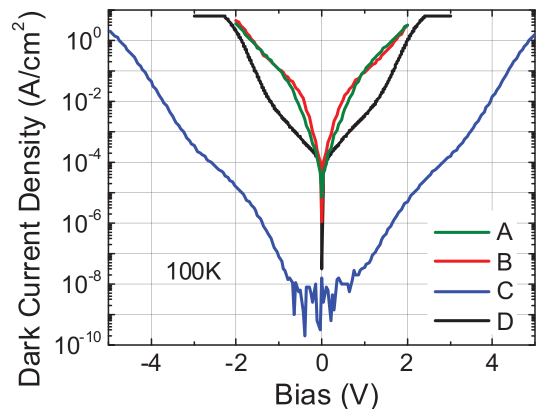

Fig. 7. Dark current density comparison between all devices at 100 K, showing several orders of magnitude reduction in the dark current for device C due to tall remote barrier. Device D also has more than an order of magnitude lower dark current as compared to devices A and B, due to the action of CE barriers.

presence of Aluminum, and is believed to be growth system dependent.

The material was processed into 410×410 μm^2 single pixel devices for top-side illumination. The mesa patterns were etched with inductively coupled plasma etching, followed by a wet chemical etching. Ge/Au/Ni/Au contact metal was deposited and annealed to form ohmic contacts. These detectors were characterized in identical conditions for comparison. Fig. 5 shows the photocurrent spectrum comparison between all four devices. As it can be seen from the schematics in Fig. 1(b) and 1(c), with the increase in the barrier energy, the excited level in the quantum well becomes more tightly confined. Due to enhanced confinement, the energy

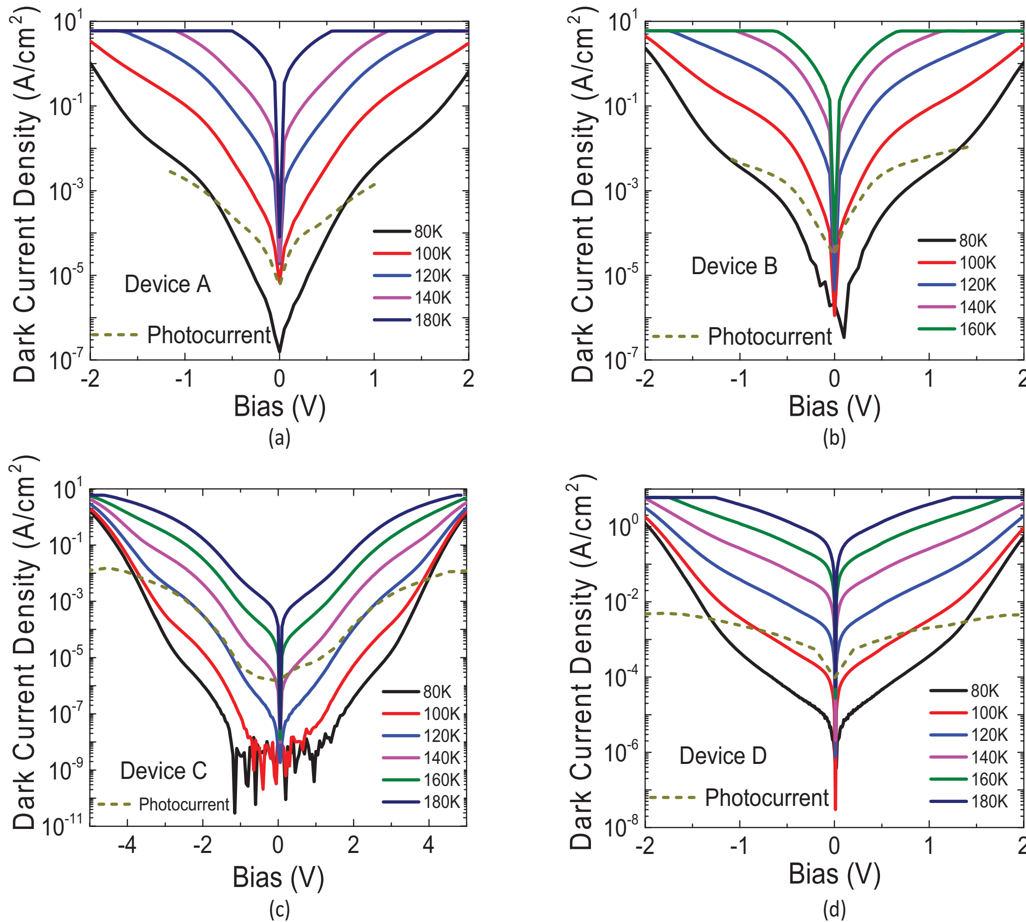

Fig. 8. Dark current density and photocurrent comparison (a) device A, (b) device B, (c) device C and (d) device D, to estimate the background limited infrared photodetection (BLIP) temperature.

separation between the two states also increases, which results in blue-shifting of the spectral response in device C. Due to larger energy step, long wavelength photoexcited electrons have poor escape probability. This results in blocking of long-wave carriers, as well as the requirement for high operating bias. This explains the spectral differences between device B and C. In device A, due to weaker confinement in the excited state, the broad midwave response, which results from bound to continuum type of transitions dominates over the longwave response. LWIR response at 10.5 μm is observable in device A and B, but with addition of $Al_{0.22}Ga_{0.78}As$ in the proximity barrier that peak is absent from device C and D. In device D, the peak at 7.55 μm comes from the transition between the first excited state in the quantum dot to the excited state in the quantum well, as suggested from the temperature dependent photocurrent spectra measurements.

Radiometric measurements were performed in liquid nitrogen cooled dewar with a calibrated blackbody setup. Fig 6(a) and (b) shows the responsivity for different proximity barriers (device A, B and D) and different remote barriers (device B and D), respectively, measured at 77K. Comparison between the responsivity of device A and B reveals that the responsivity of device A is lower than device B by close to an order of magnitude. For example, at a bias of 0.5V, the responsivity of device A is 13mA/W while that of device B is 110 mA/W. This increase in the responsivity, for a same remote barrier and a similar spectral range is attributed to the increase in confinement due to higher energy proximity barrier. This trend continues, at lower biases, between device B and D, as highlighted in Table I. Due to confinement enhancing action of $Al_{0.22}Ga_{0.78}As$ CE-barriers, the responsivity is higher than device B, in the lower bias range. At higher bias, however, the device D starts saturating before device B, due to closeness of excited level in device D with respect to the remote barrier, as shown in Fig. 1. Fig. 5(b) reveals the effect of remote barrier on the responsivity. Device C has lowest responsivity at a given bias, but the bias range is much higher than other devices. The bias range in these measurements was limited by saturation of the preamplifier used to collect the current output. The lower responsivity, by a few orders of magnitude, in device C is a result of large energetic barrier provided by thick $Al_{0.22}Ga_{0.78}As$ remote barrier. This barrier blocks photocurrent carriers as well as dark current carriers, resulting in low responsivity as well as low dark current, as discussed later. These comparisons clearly indicate that the increase in the energy of the proximity barrier increases the responsivity, before it starts saturating at higher biases, while increase in the remote barrier drastically reduces the responsivity, and increases the operating bias range.

Fig. 7 compares the dark current densities obtained from all the four devices at 100K. As can be clearly seen, device C has more than five orders of magnitude lower dark current than

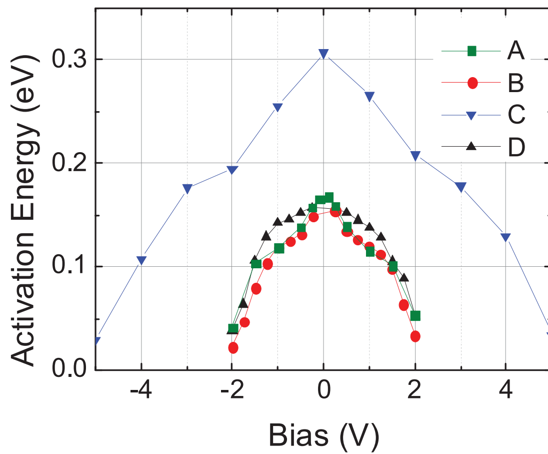

Fig. 9. Activation energy for the four devices confirming the proximity barrier's small effect and the remote barrier's large effect on the activation energy.

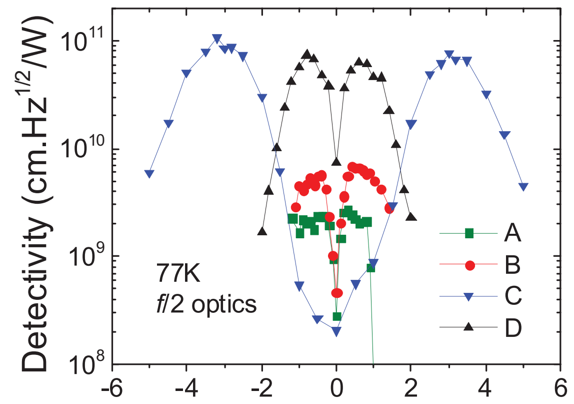

Fig. 10. Comparison of detectivities of all four devices at 77 K. This clearly shows that the increase in the proximity barrier energy increases the detectivity due to increase in signal and decrease in noise. This does not add to the operating bias for maximum detectivity. Device C, due to the presence of the large remote barrier, has high detectivity due to low dark current, but it needs large bias voltage for optimum performance.

device D, which has a same proximity barrier but different remote barrier. This reduction is more than the reduction in the responsivity, as seen before, thus the overall signal to noise ratio is maintained high. Comparison between dark current density of device A and B reveals that the effect of increase in the barrier height for the proximity barrier on the dark current levels is negligible. However, device D has more than an order of magnitude lower dark current as compared to device A and B, as the proximity barrier is at higher energy than the remote barrier, which blocks some of the dark current carriers. Thus, the effect of CE barrier is to increase the responsivity while simultaneously lowering the dark current, thus increasing the overall signal to noise ratio.

Comparison of the dark current densities and photocurrent densities for all the samples at different temperatures is shown in Fig. 8(a)-(d). The photocurrent density was calculated by multiplying incident number of photons per second on the detector with the conversion efficiency of the detector, calculated from the measured responsivity. Responsivity value at 77K was used, as the change in responsivity with the increase in temperature is small. Comparison reveals that the background limited infrared photodetection (BLIP) condition is satisfied below 80K for device A and device B, 100K for device C and device D, at the optimum operating bias. The activation energies calculated from this data is plotted in Fig. 9. It shows that the activation energy is only weakly dependent on the composition of the proximity barrier, while is a strong function of the remote barrier energy. By changing the remote barrier to $Al_{0.22}Ga_{0.78}As$ from $Al_{0.07}Ga_{0.93}As$, the activation energy is increased by approximately 150 meV (bias dependent), which corresponds to increase in the barrier height. This is to be expected as the activation energy is approximately the difference between the barrier energy and the Fermi energy.

The most important figure of merit from the detector operation point of view is specific detectivity, which is the normalized signal to noise ratio. Fig. 10 compares the detectivity of all the four devices at 77K for $f/2$ optics. It is to be noted that the detectivity is underestimated at low bias in device C (from −2V to 2V) and D (from −0.4V to 4V) due to the system noise limit on the noise measurement. As expected, the detectivity increases from device A to device B, due to increase in responsivity. Device C has much higher detectivity as compared to device B, an order of magnitude increase. However, the peak detectivity is at −3V, which is too large bias for the FPA operation, due to limitations of typical ROICs. Device D, however, combines the best of both the worlds, with high detectivity at a low bias. It is to be noted that device D has a longer peak wavelength than device C.

IV. Conclusion

In conclusion, effects of proximity barrier and remote barrier on the device performance are very different in nature. As the proximity barrier energy increases, the confinement in the excited state of DWELL region increases, which leads to an increase in the wavefunction overlap with the ground state, thus increasing the responsivity, before it starts saturating at higher bias for large proximity barrier. The growth mechanism assures that the confinement enhancing barriers have been grown conformally over the quantum dot regions, as confirmed by RHEED and TEM images. Proximity barrier higher than the remote barrier, such as in device D, also leads to a dramatic reduction in dark current. The activation energy only weakly depends on the proximity barrier. On the contrary, as the remote barrier energy increases, both signal and dark currents are drastically reduced, the peak wavelength is blueshifted, and the activation energy is proportionally increased. This leads to high detectivities, but the optimum operating bias is also increased. Thus, with high detectivity, high responsivity, lower dark current, excellent optical quality of quantum dots and operation at low bias voltage suitable for focal plane array applications, device D, with CE-DWELL configuration optimizes the performance as it combines the advantages of large proximity barrier and small remote barrier.

REFERENCES

[1] A. V. Barve and S. Krishna, “Quantum dot infrared photodetectors,” in *Advances in Infrared Photodetectors*, vol. 84, S. D. R. D. R. J. C. Gunapala, Ed. New York: Academic, 2011, pp. 153–193.

[2] J. C. Campbell and A. Madhukar, “Quantum-dot infrared photodetectors,” *Proc. IEEE*, vol. 95, no. 9, pp. 1815–1827, Sep. 2007.

[3] E. T. Kim, A. Madhukar, Z. M. Ye, and J. C. Campbell, “High detectivity InAs quantum dot infrared photodetectors,” *Appl. Phys. Lett.*, vol. 84, pp. 3277–3279, Apr. 2004.

[4] S. Chakrabarti, A. D. Stiff-Roberts, X. H. Su, P. Bhattacharya, G. Ariyawansa, and A. G. U. Perera, “High-performance mid-infrared quantum dot infrared photodetectors,” *J. Phys. D, Appl. Phys.*, vol. 38, pp. 2135–2141, Jul. 2005.

[5] J. Jiang, S. Tsao, T. O’Sullivan, W. Zhang, H. Lim, T. Sills, K. Mi, M. Razeghi, G. J. Brown, and M. Z. Tidrow, “High detectivity InGaAs/InGaP quantum-dot infrared photodetectors grown by low pressure metalorganic chemical vapor deposition,” *Appl. Phys. Lett.*, vol. 84, no. 12, pp. 2166–2168, 2004.

[6] S. Tsao, H. Lim, H. Seo, W. Zhang, and M. Razeghi, “InP-based quantum-dot infrared photodetectors with high quantum efficiency and high-temperature imaging,” *IEEE Sensors J.*, vol. 8, no. 6, pp. 936–941, Jun. 2008.

[7] A. Stintz, G. T. Liu, A. L. Gray, R. Spillers, S. M. Delgado, and K. J. Malloy, “Characterization of InAs quantum dots in strained $In_xGa_{1-x}As$ quantum wells,” *J. Vac. Sci. Technol. B*, vol. 18, no. 3, pp. 1496–1501, May–Jun. 2000.

[8] S. Krishna, “Quantum dots-in-a-well infrared photodetectors,” *J. Phys. D, Appl. Phys.*, vol. 38, pp. 2142–2150, Jul. 2005.

[9] S. Krishna, S. Raghavan, G. V. Winckel, A. Stintz, G. Ariyawansa, S. G. Matsik, and A. G. U. Perera, “Three-color ($\lambda_{p1} \sim 3.8\ \mu$m, $\lambda_{p2} \sim 8.5\ \mu$m, and $\lambda_{p3} \sim 23.2\ \mu$m) InAs/InGaAs quantum-dots-in-a-well detector,” *Appl. Phys. Lett.*, vol. 83, no. 14, pp. 2745–2747, 2003.

[10] P. Rotella, G. V. Winckel, S. Raghavan, A. Stintz, Y. Jiang, and S. Krishna, “Study of structural and optical properties of quantum dots-in-a-well heterostructures,” *J. Vac. Sci. Technol. B, Microelectron. Nanometer Struct.*, vol. 22, no. 3, pp. 1512–1514, May 2004.

[11] P. Aivaliotis, S. Menzel, E. A. Zibik, J. W. Cockburn, L. R. Wilson, and M. Hopkinson, “Energy level structure and electron relaxation times in InAs/$In_xGa_{1-x}As$ quantum dot-in-a-well structures,” *Appl. Phys. Lett.*, vol. 91, no. 25, pp. 253502-1–253502-3, 2007.

[12] G. Jolley, L. F. H. H. Tan, and C. Jagadish, “Influence of quantum well and barrier composition on the spectral behavior of InGaAs quantum dots-in-a-well infrared photodetectors,” *Appl. Phys. Lett.*, vol. 91, no. 17, pp. 173508-1–173508-3, Oct. 2007.

[13] E.-T. Kim, Z. Chen, and A. Madhukar, “Tailoring detection bands of InAs quantum-dot infrared photodetectors using $In_xGa_{1-x}As$ strain-relieving quantum wells,” *Appl. Phys. Lett.*, vol. 79, no. 20, pp. 3341–3343, 2001.

[14] T. E. Vandervelde, M. C. Lenz, E. Varley, A. Barve, J. Shao, R. V. Shenoi, D. A. Ramirez, W. Jang, Y. D. Sharma, and S. Krishna, “Quantum dots-in-a-well focal plane arrays,” *IEEE J. Sel. Topics Quantum Electron.*, vol. 14, no. 4, pp. 1150–1161, Jul.–Aug. 2008.

[15] R. V. Shenoi, R. S. Attaluri, A. Siroya, J. Shao, Y. D. Sharma, A. Stintz, T. E. Vandervelde, and S. Krishna, “Low-strain InAs/InGaAs/GaAs quantum dots-in-a-well infrared photodetector,” *J. Vac. Sci. Technol. B, Microelectron. Nanometer Struct.*, vol. 26, no. 3, pp. 1136–1139, May 2008.

[16] A. Barve, J. Shao, Y. D. Sharma, T. E. Vandervelde, K. Sankalp, S. J. Lee, S. K. Noh, and S. Krishna, “Resonant tunneling barriers in quantum dots-in-a-well infrared photodetectors,” *IEEE J. Quantum Electron.*, vol. 46, no. 7, pp. 1105–1114, Jul. 2010.

[17] S. D. Gunapala, S. V. Bandara, C. J. Hill, D. Z. Ting, J. K. Liu, S. B. Rafol, E. R. Blazejewski, J. M. Mumolo, S. A. Keo, S. Krishna, Y. C. Chang, and C. A. Shott, “640×512 pixels long-wavelength infrared (LWIR) quantum-dot infrared photodetector (QDIP) imaging focal plane array,” *IEEE J. Quantum Electron.*, vol. 43, no. 3, pp. 230–237, Mar. 2007.

[18] G. Jolley, L. Fu, H. H. Tan, and C. Jagadish, “Effects of well thickness on the spectral properties of $In_{0.5}Ga_{0.5}As/GaAs/Al_{0.2}Ga_{0.8}As$ quantum dots-in-a-well infrared photodetectors,” *Appl. Phys. Lett.*, vol. 92, no. 19, pp. 193507-1–193507-3, 2008.

[19] A. V. Barve, T. Rotter, Y. Sharma, S. J. Lee, S. K. Noh, and S. Krishna, “Systematic study of different transitions in high operating temperature quantum dots in a well photodetectors,” *Appl. Phys. Lett.*, vol. 97, no. 6, pp. 061105-1–061105-3, Aug. 2010.

[20] A. V. Barve, J. Montaya, Y. Sharma, T. Rotter, J. Shao, W.-Y. Jang, S. Meesala, S. J. Lee, and S. Krishna, “High temperature operation of quantum dots-in-a-well infrared photodetectors,” *Infr. Phys. Technol.*, vol. 54, pp. 215–219, May 2011.

[21] A. V. Barve, S. Sengupta, J. O. Kim, Y. D. Sharma, S. Adhikary, T. J. Rotter, S. J. Lee, Y. H. Kim, and S. Krishna, “Confinement enhancing barriers for high performance quantum dots-in-a-well infrared detectors,” *Appl. Phys. Lett.*, vol. 99, no. 19, pp. 191110-1–191110-3, 2011.

Ajit V. Barve (S’08) received the B.S. degree from the University of Mumbai, Mumbai, India, in 2005, the M.S. degree in electrical engineering from the Indian Institute of Technology, Kanpur, India, in 2007, and the Ph.D. degree from the Center for High Technology Materials, University of New Mexico, Albuquerque, in 2012.

He is currently with the Department of Electrical and Computer Engineering, University of California Santa Barbara, Santa Barbara. His current research interests include optoelectronics, with a focus on epitaxial growth, fabrication, and characterization of devices. His experience in research includes infrared detectors and vertical cavity surface emitting lasers.

Dr. Barve is a member of LEOS and SPIE societies.

Saumya Sengupta received the B.Sc. (Hons.) degree in physics from the University of Calcutta, Kolkata, India, in 2006, and the M.Sc. degree in applied physics from the Indian School of Mines, Dhanbad, India, in 2008. He is currently pursuing the Ph.D. degree with the Indian Institute of Technology Bombay, Mumbai, India.

His current research interests include molecular beam epitaxy grown III–V semiconductor materials and quantum dot infrared photodetectors.

Jun Oh Kim received the B.S. degree in electrical engineering and the M.S. and Ph.D. degrees in physics from Kyunghee University, Yongin-Si, Korea, in 2004, 2006, and 2010, respectively.

He was a Researcher with the Korea Research Institute of Standards and Science, Daejeon, Korea, from 2004 to 2010. He is currently with the Center for High Technology Materials, University of New Mexico, Albuquerque. His current research interests include the epitaxial growth, fabrication, and characterization of the quantum dots infrared photodetectors.

John Montoya received the Bachelor of Science degree in electrical engineering from the New Mexico Institute of Mining and Technology, Socorro, in 2006, and the Master of Science degree in electrical engineering from the University of Missouri-Rolla, Rolla, in 2008. He is currently pursuing the Doctorate degree in nanoscience and microsystems with the University of New Mexico, Albuquerque.

He is currently involved in research on the development of high Q-factor photonics crystals to enhance the quantum efficiency of infrared photodetectors with the University of New Mexico. His current research interests include photonics detectors, computational electrodynamics, and quantum theory.

Mr. John is a fellow of the NSF-sponsored IGERT Program on Nanoscience and Microsystems.

Brianna Klein received the B.S. and M.S. degrees in electrical engineering from the New Mexico Institute of Mining and Technology, Socorro, in 2008 and 2009, respectively. Her M.S. thesis focused primarily on building and characterizing sensors for instrumenting a Ranque-Hilsch Tube. She is currently pursuing the Ph.D. degree in electrical engineering with the Center for High Technology Materials, University of New Mexico, Albuquerque.

Her current research interests include basic properties of Type II InAs- and GaSb-strained layer superlattices, including carrier lifetime, absorption characteristics, carrier mobility, and defect levels.

Mohammad Ali Shirazi (S'12) received the B.Sc. degree in electrical engineering from the University of Tehran, Tehran, Iran, in 2009. He is currently pursuing the M.Sc. degree in optical science and engineering with a focus on photonics with the University of New Mexico, Albuquerque.

His current research interests include photonic integrated circuits, III–V and organic semiconductor devices, plasmonics, and metamaterials.

Dr. Shirazi-HD was the recipient of the First Place Award of the Student Design Competition at the IEEE MTT-S International Microwave Symposium, Anaheim, CA, in 2010.

Marziyeh Zamiri received the B.S. degree in electrical engineering from the Isfahan University of Technology, Isfahan, Iran, in 2006, and the Masters degree in photonics. She started to pursue the Ph.D. degree with Ohio State University, Columbus, while researching the thermoelectric properties of SiGe n-type, in 2010, and then transferred to the University of New Mexico, Albuquerque, and joined the Krishna's Group, in 2011.

She was engaged in research on the influence of electrically conductive cap layers, such as silver, on the magnetoimpedance effect in Co68.15 Fe4.35 Si12.5 B15 ribbons with the Nanomagnetics and Magnetic Semiconductors Laboratory, Laser Research Institute, Shahid Beheshti University, Tehran, Iran, during her Masters study. She is currently researching GaAs substrate removal and quantum dot design for quantum dot infrared detectors.

Yagya D. Sharma (SM'01) received the Master of Philosophy degree in material science from the Indian Institute of Technology Roorkee, Roorkee, India, in 1992, and the Ph.D. degree in electronics science from the University of Delhi, New Delhi, India, in 2003.

He was with the Department of Electronics Engineering, University of Osaka, Osaka, Japan, from 2004 to 2006, under the Ministry of Education, Culture, Sports, Science and Technology Japanese Government Research Fellowship, where he was engaged in research on integrated distributed feedback semiconductor lasers. He is with the Center for High Technology Materials, University of New Mexico, Albuquerque, where he is engaged in research on strain layer superlattice and quantum dot infrared detectors. He has authored or co-authored more than 65 papers published in peer-reviewed journals and international conferences. His current research interests include metamaterial and plasmonic structure, GaSb and GaAs-based infrared detectors, and focal plane arrays.

Dr. Sharma is a Senior Member of the Lasers and Electro-Optics Society. He is also a member of the International Society for Optical Engineers, the Optical Society of America, the Materials Research Society, and is a Life Member of the Semiconductor Society of India.

Sourav Adhikary received the B.Sc. (Hons.) degree in physics from the Scottish Church College, University of Calcutta, Kolkata, India, and the M.Sc. degree in applied physics from the Indian School of Mines, Dhanbad, India, in 2008. He is currently pursuing the Ph.D. degree in electrical engineering with the Indian Institute of Technology Bombay, Mumbai, India, where he is researching InAs- and GaAs-based materials and quantum-dot infrared photodetectors.

Sebastián E. Godoy was born in Concepción, Chile. He received the B.Sc. and M.Sc. degrees in electrical engineering from the University of Concepción, Concepcion, Chile, in 2006 and 2009, respectively. He is currently pursuing the Ph.D. degree in electrical engineering at the Center for High Technology Materials, University of New Mexico, Albuquerque.

He has been an Academic Collaborator with the University of Concepción since 2007. He is sponsored by the University of Concepción and the Comisión Nacional de Investigación Científica y Tecnológica, Chile, under the Program "Becas Chile."

Woo-Yong Jang received the B.E. (Hons.) degree in from the University of Canterbury, Ilam, New Zealand, in 2001, and the M.S. degree from the University of Southern California, Los Angeles, in 2004, both in electrical engineering. He is currently pursuing the Ph.D. degree in electrical and computer engineering with the University of New Mexico, Albuquerque, where he is currently a graduate student with the Center for High Technology Materials.

Glauco R. C. Fiorante received the B.S. degree in electrical engineering from Santa Cecilia University, Santos, Brazil, in 1995, and the M.S. degree in electrical engineering from the University of Sao Paulo, Sao Paulo, Brazil, in 2004. He is currently pursuing the Ph.D. degree in microelectronics with the Center for High Technology Materials, University of New Mexico, Albuquerque.

He has been a Professor with the Electrical and Computer Department, Federal Institute of Education, Sciences and Technology of Sao Paulo-IFSP-SP, Brazil, since 1995. He was engaged for seven years with petrochemical and manufacturing industries as a Research and Development Engineer of embedded systems at Sao Paulo, Brazil. His current research interests include electron multiplying charge-coupled devices and applications, very large scale-integrated (VLSI) read-out integrated circuits for focal plane arrays and embedded systems for image acquisition and processing, and VLSI integrated circuits testing. Prof. Glauco is a fellow of the CAPES-Ministry of Education-Brazil and FULBRIGHT.

Subhananda Chakrabarti (M'06) received the M.Sc. and Ph.D. degrees from the Department of Electronic Science, University of Calcutta, Kolkata, India.

He was a Lecturer in physics with St. Xavier's College, Kolkata. He was a Senior Research Fellow with the University of Michigan, Ann Arbor, from 2001 to 2005, a Senior Researcher with Dublin City University, Dublin City, Ireland, from 2005 to 2006, and a Senior Researcher (RA2) with the University of Glasgow, Glasgow, U.K., from 2006 to 2007. He joined the Department of Electrical Engineering, IIT Bombay, Mumbai, India, in 2007. He has extensively researched molecular beam epitaxial growth, characterization, and fabrication of semiconductor optoelectronic materials and devices, such as quantum dot laser, intersubband detectors, vertical cavity surface and emitting lasers. He has authored or co-authored more than 160 papers in journals and conferences. He has also co-authored a couple of book chapters on intersubband quantum dot detectors.

Dr. S. Chakrabarti is a Reviewer of the IEEE PHOTONICS TECHNOLOGY LETTERS, the IEEE JOURNAL OF QUANTUM ELECTRONICS, and the Material Research Bulletin.

Sanjay Krishna (S'98–M'01–SM'00) received the Masters degree in physics from the Indian Institute of Technology Madras, Chennai, India, in 1996, the M.S. degree in electrical engineering in 1999, and the Ph.D. degree in applied physics from the University of Michigan, Ann Arbor, in 2001.

He joined the University of New Mexico, Albuquerque, as a Tenure Track Faculty Member in 2001, where he is currently a Professor with the Electrical and Computer Engineering Department, Center for High Technology Materials. He has authored or co-authored more than 200 peer-reviewed journal articles (h-index = 29) and holds six issued patents. His current research interests include growth, fabrication, and characterization of self-assembled quantum dots and Type_II InAs- and InGaSb-based strain layer superlattices for midinfrared detectors.

Prof. Krishna is a fellow of SPIE. He was the recipient of various awards, including the Gold Medal from the IIT Madras, the Early Career Achievement Award from the SPIE, NAMBE and IEEE-Nanotechnology Council, and the UNM Teacher of the Year Award.